LBL-29551

Lawrence Berkeley Laboratory
UNIVERSITY OF CALIFORNIA

Physics Division

Submitted to Astrophysical Journal

Mayflower Mine 1.5 TV Detector: Cosmic Ray Anisotropy and Search for Cygnus X-3

D.J. Cutler and D.E. Groom

September 1990

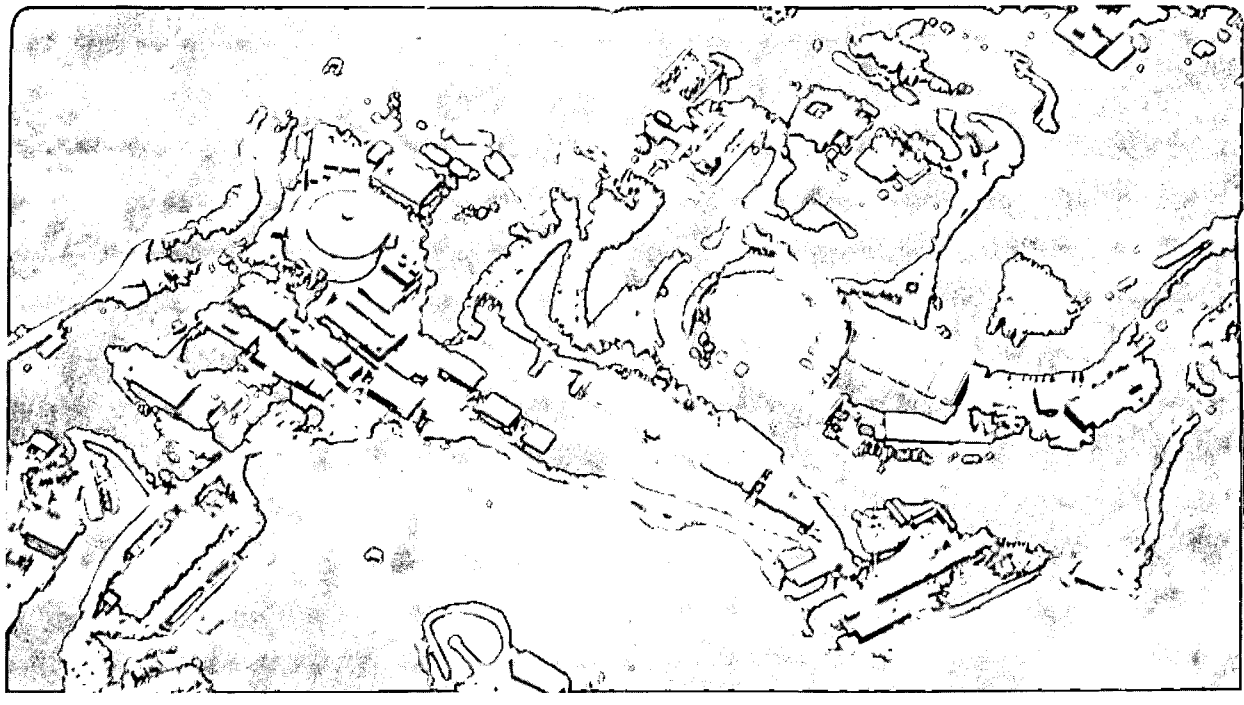

Prepared for the U.S. Department of Energy under Contract Number DE-AC03-76SF00098

DISCLAIMER

LBL–29551

MAYFLOWER MINE 1.5 TV DETECTOR: COSMIC RAY ANISOTROPY AND SEARCH FOR CYGNUS X-3*

D. J. CUTLER† AND D. E. GROOM‡

Physics Department, University of Utah

28 September 1990

Submitted to *The Astrophysical Journal*

---

* This work was supported, in part, by National Science Foundation grants AST80-10727 and PHY83-08135, administered by the University of Utah. Publication at Lawrence Berkeley Laboratory was supported by Department of Energy Contract No. DE-AC03-76SF00098.

† Present address: Spectrum Systems, Spokane, Washington.

‡ Present address: Lawrence Berkeley Laboratory, Berkeley, California.

MAYFLOWER MINE 1.5 TV DETECTOR: COSMIC RAY ANISOTROPY AND SEARCH FOR CYGNUS X-3

D. J. CUTLER[1] AND D. E. GROOM[2]

Physics Department, University of Utah

ABSTRACT

An underground muon detector was used to search for periodic changes in the cosmic-ray flux over a 5.4 year period terminating in 1983 May. Primary cosmic rays with a median rigidity of 1.5×10^{12} V produced a 4.4 Hz muon rate. The Fourier transformed data show a peak at the sidereal frequency with relative amplitude $(3.2^{+0.8}_{-0.6}) \times 10^{-4}$, which after correction for solar motion with respect to the local interstellar medium indicates an anisotropy of $(5.3^{+0.8}_{-0.7}) \times 10^{-4}$ at right ascension $3^{h}.2 \pm 0.5$. We also observe a second harmonic with amplitude $(2.9^{+0.9}_{-0.7}) \times 10^{-4}$ at $\alpha = 8^{h}.4 \pm 1^{h}.1$ and a third harmonic with amplitude $(2.1^{+0.8}_{-0.6}) \times 10^{-4}$ at $\alpha = 0^{h}.0 \pm 1^{h}.2$. The amplitude and phase of the signal at the solar frequency are those expected from the earth's orbital motion. A search at the 5.01 day^{-1} Cyg X-3 frequency yielded no robust signal.

Subject headings: cosmic rays: general

I. INTRODUCTION

We have monitored the muon rate 500 hg^{-1}cm^2 underground for 5.4 years in order to measure the sidereal anisotropy of cosmic rays trapped in the magnetic fields of the galactic disk. The detector operated 64% of the time between 1978 January and 1983 May, and recorded 4.7×10^8 muon events.

An analysis based on approximately half of the data was published earlier (Cutler, Bergeson, Davis, and Groom 1981; hereafter CBDG). The new results

[1] Present address: Spectrum Systems, Spokane, Washington.

[2] Present address: Lawrence Berkeley Laboratory, Berkeley, California.

confirm and improve those reported earlier. All reported effects have persisted and are visible in the new data alone. In the combined data errors are smaller, and the peaks are narrower in the Fourier transforms at the critical frequencies. In addition, a somewhat marginal signal was observed at the solar frequency which agreed in amplitude and phase with that expected from the orbital motion of the earth (Cutler and Groom 1986). About 10% of the detector was used for a monopole search (Groom *et al.* 1983). A group operating at the same time in the Soudan Mine reported a muon signal correlated with the source Cyg X-3 (Marchak *et al.* 1985), so Mayflower data were reanalyzed to search for such a signal (Cutler and Groom 1987). In this paper we report the new sidereal results and the Cyg X-3 search results. Since the strategy, apparatus, and analysis technique were thoroughly reported in CBDG, only summary descriptions are provided here.

The subject of the study is that part of the cosmic-ray plasma which is presumably injected into the interstellar medium by sources within the galaxy and which remains trapped by the galactic magnetic fields until its eventual escape. In practical terms, this means cosmic rays that have cyclotron radii much smaller than the thickness of the galactic disk (rigidities[1] much smaller than 10^4–10^5 TV) but are sufficiently rigid that they reach the earth without severe disruption by the solar fields (rigidities larger than a few hundred GV). Since the cosmic-ray intensity is a rapidly falling function of energy, it is convenient and economical to make measurements at the lowest energy free of solar effects. For this experiment the depth was chosen so that the progenitors of the observed muons had a median rigidity of about 1.5 TV.

The experiment was originally motivated by an apparent discrepancy between the near-anisotropy of galactic cosmic rays and the very short lifetime inferred from their composition. The relative abundance of spallation products (Li, Be, B) indicates that low-energy cosmic rays have passed through only 5–10 g cm^{-2} of interstellar matter, or a residence time of about 10^6 yr in the galactic disk

1 Rigidity is the momentum per *charged* nucleon, p/Z, where p is the total momentum measured e.g. in TeV/c ≡TV.

(Daniel and Stevens 1975, Shapiro 1982). With any reasonable field configuration the plasma would then stream toward escape holes at an easily observable velocity. Many of the experiments reported at the time had very low threshold energies, and some were questionable for other reasons (discussion and references in CBDG). Even before CBDG, partial resolution had come from several sources: Measurements of the ^{10}Be ($t_{1/2} = 1.6 \times 10^6$ yr) relative abundance (Hagan, Fisher, and Ormes 1977; Garcia-Munoz, Mason, and Simpson 1977; Wiedenbeck and Greiner 1980) indicated a cosmic-ray lifetime close to 1×10^7 yr. From this lifetime and the spallation-product abundances, it can be inferred that the cosmic rays spend $\sim 80\%$ of this time outside the galactic disk. At the same time several high-energy and high-quality anisotropy measurements were published (Fenton and Fenton 1975, 1976, at Poatina, Tasmania; Gomboshi *et al.* 1975*a*, *b* at Musala Peak in Hungary, and Sakakibara *et al.* 1979 at Mt. Norikura, Japan) which agreed in amplitude (after correction for latitude) and phase. High-statistics results by Davies, Elliot, and Thambyahpilla (1976, in London) also agree in spite of low (600 GV) median primary rigidity.

A simple streaming of the cosmic ray plasma would lead only to a dipole moment in the intensity distribution, or a first harmonic in the intensity as scanned by the earth's rotation. Along with the Norikura and Musala groups, we reported the puzzling presence of a second harmonic, and in this paper report a third. Higher harmonics can be used to unravel declination information only if information from detectors at very different latitudes is available. The Poatina experiment is thus the only candidate, and its error bars are consistent with the reported absence of a second harmonic. An improved southern-hemisphere experiment is thus needed to complete the picture.

II. STRATEGY

The cosmic-ray intensity is known to be nearly isotropic at energies small compared with 10^{16} eV, so in the assumed absence of narrow-angle features the intensity can be represented by the first few terms of an expansion in spherical har-

monics. With the additional assumption of symmetry about the local interstellar magnetic-field direction (Nagashima *et al.* 1972; Király *et al.* 1979), this expansion becomes

$$I(\psi)/\langle I\rangle = 1 + \sum \eta_\ell P_\ell(\cos\psi) \ , \tag{2.1}$$

where P_ℓ is the Legendre polynomial of order ℓ and ψ is the polar angle measured away from the symmetry axis or field direction. This axis is taken as pointing toward the direction (α, δ) of the first harmonic maximum, so that the amplitude η_1 is positive. It is known in advance that η_1 is a few times 10^{-4}, and it is expected that the series is rapidly convergent. These statements imply that $O(10^8)$ events per year must be observed in a useful experiment, and that extreme angular resolution is not of the essence.

Nagashima *et al.* (1989) have developed expansions similar to that given in Eq. 2.1, but have not taken advantage of the simplicity introduced by the symmetry axis.

In practice, a fixed detector at effective latitude λ scans the sky at the sidereal frequency $\omega_\star$, recording a time-varying signal given by

$$I(t)/\langle I\rangle = 1 + \sum \xi_m \cos m(\omega_\star t - \varphi_m) \ . \tag{2.2}$$

Since

$$\cos\psi = \sin\lambda\sin\delta + \cos\lambda\cos\delta\cos(\omega_\star t + \alpha_0 - \alpha) \tag{2.3}$$

for a detector pointing at α_0 at $t = 0$, the ξ_m and η_ℓ can be related:

$$\xi_m = \sum_{\ell=m}^{\infty} C_{m\ell}(\lambda,\delta)\eta_\ell \tag{2.4}$$

All time harmonics should have the same phase $\varphi_m = \alpha_0 - \alpha$, modulo $2\pi/m$, with the proper choice of signs for the ξ_m. Graphs of the low-order $C_{m\ell}(\lambda,\delta)$ are given

in CBDG. The first two coefficients are given by

$$\begin{aligned} \xi_1 &= \eta_1 \cos\lambda \cos\delta + 3\,\eta_2 \cos\lambda \sin\lambda \cos\delta \sin\delta + \ldots \\ \xi_2 &= \tfrac{3}{4}\eta_2 \cos^2\lambda \cos^2\delta + \ldots \end{aligned} \tag{2.5}$$

where terms of order η_ℓ^2 have been dropped.

If an observer moves with velocity v with respect to the rest frame of a cosmic-ray plasma with energy spectrum $E^{-\gamma}$,

$$\eta_1 = (2+\gamma)(v/c) \tag{2.6}$$

(Compton and Getting 1935; Gleeson and Axford 1968), and in our energy region $\gamma \approx 2.7$. The first harmonic can thus be understood as a measure of the bulk streaming velocity of the plasma, while higher harmonics represent more complicated streaming. For example, the negative η_2 which we report means inflow in the equatorial plane ($\psi = \pi/2$) and outflow at the poles. We also note from the above relationships that

a) If only η_1 exists, no declination information is available, even from an ensemble of experiments at different latitudes.

b) Even if η_1 vanishes, a temporal first harmonic ξ_1 can exist; it will change sign (or phase) for an experiment in a different hemisphere.

c) These statements are strictly true only in the rest frame of the local interstellar medium (LISM). If the sun moves with velocity v toward (α_I, δ_I), a term

$$(2+\gamma)(v/c) \cos\lambda \cos\delta \cos(\omega_\star t - \alpha_I) \tag{2.7}$$

must be added to the right side of Eq. (2.2). A similar correction for the earth's motion appears at the solar frequency.

III. DETECTOR

An underground muon detector was chosen because of its inherent stability and relative ease of data interpretation. The problem of relating its muon energy threshold (depth underground) to a primary cosmic-ray rigidity distribution has been addressed by Gaisser (1974, 1976), Groom and Morrison (1975), and by Murakami *et al.* (1976). More recent data for their assumed scaling models is now available from the S$\bar{\text{p}}$pS and Tevatron, but it mainly verifies the correctness of their extrapolations. Following Gaisser (1976), we take 10.4 as the factor relating muon energy threshold E_μ to median proton energy $E_{\rm med}$ at our energy. If 80% of the cosmic rays arrive as protons, then the median primary rigidity is 1.17 times greater.

The requirement $R_{\rm med} > 1$ TV, or $E_\mu > 82$ GeV, resulted in a search which led to the recently-closed Mayflower Mine, near Heber, Utah, at 40°37′ N, 111°27′ W. Not far from the entrance, the nearly east-west main drift was at an intensity-weighted average depth of 507 hg cm^{-2}, corresponding to $\langle E_\mu \rangle = 128$ GeV, or $R_{\rm med} = 1500$ GV. Because of the shape of the overburden, the effective latitude and longitude of the detector were 41°.7 N and 110°.8 W.

The detector consisted of 300 plastic scintillation counters arranged in three layers, each with area 37 m^2, separated by 75 g cm^{-2} of concrete. Each counter was 25 cm wide, and most were 150 cm long. They were arranged with their long axes in the north-south direction, resulting in a 15° right ascension resolution for vertical muons triggering three layers.

The addresses of triggered counters were read after each coincident trigger of all three planes. Simple pattern recognition was performed on-line, while complicated events were recorded verbatim for off-line analysis. In spite of the loose trigger, 96% of the triggers were associated with unambiguous single muons. Data were collected for 65% of the 5.4 year interval between 1978 Jan 5 and late 1983 May for a total of 4.7×10^8 events. These were tallied in 60,419 non-empty half-hour summaries, with an average of 7810 events per summary. Ancillary records concerning various

voltages in the system, temperature, etc. were also written, as described in CBDG.

IV. DATA PROCESSING

The single-muon data were re-binned into uniformly spaced intervals of length Δt, usually chosen as two hours for the anisotropy measurements. Different counter combinations viewed different parts of the sky; the various sectors were rebinned with appropriate phasing. Rates were corrected for inefficiency in the rare case of a broken or suspicious counter, and for the 10% smaller detector in use after the start of the monopole search.

The variable actually used in the signal-processing algorithms was the fractional deviation from the average muon intensity. For the nth interval of length Δt, it is given by

$$x(n\Delta t) = \left[I(n\Delta t) - \langle I \rangle\right] / \langle I \rangle \ . \tag{4.1}$$

Zeros were inserted where no data existed. Detrending algorithms were normally used to further condition the x_n. The chief effect of such detrending was the suppression of low-frequency noise, but since the tail of this distribution did contribute to the noise near $(1 \text{ day})^{-1}$, some overall improvement was obtained. Typically, $\langle I \rangle$ was taken as the 3-day running average of the data.

Both discrete Fourier transform (DFT) and fast Fourier transform (FFT) algorithms were used. The one-sided DFT was defined as

$$X(f) = \frac{2}{M} \sum_{n=0}^{N-1} x(n\Delta t) e^{-2\pi i f n \Delta t} \ , \tag{4.2}$$

where

$M =$ number of non-empty data points (60,419 if half-hour bins are used);

$N =$ number of points in the transform, typically 2^{17};

$\Delta t =$ time interval for each point;

$f =$ frequency. With this definition, the norm of X at the mth sidereal harmonic is the ξ_m introduced in Equation 2.2. The norm $|X(f)|$ rather than the more conventional power $|X(f)|^2$ is used throughout, so that the scales are linear in the quantities of interest.

The DFT of the data window is shown in Fig. 1. It should represent the line shape of a stationary feature in the data. The intricate sidelobe structure is the result of gaps in the data string. The width of the peak should be roughly given by the inverse of the length of the data string, and it will be seen from a comparison with Fig. 3 of CBDG that the peak is half as wide for the full data set. It is important that the peak width be small compared with the separation between interesting frequencies (*e.g.* 0.0027 day^{-1} between solar and sidereal first harmonics), since this guarantees the lack of contamination of signals from those at nearby frequencies.

For an experiment of this sort, the real and imaginary parts of $X(f)$ distribute normally about their respective means with standard deviations $\sigma_0 = \sqrt{2/\mathcal{N}}$, where $\mathcal{N}$ is the total number of muon events in the experiment. Unfortunately, the norm is the quantity of interest. If means are known to vanish, then the norm $\xi = |X|$ obeys the Rayleigh distribution, $-(d/d\xi)[\exp(-\xi^2/2\sigma_0^2)]$. Our estimates of σ are obtained from fits to this function using data from a small frequency range near frequencies of interest. Near the first harmonic the fitted values are about 12% larger than σ_0 because of contamination from low-frequency noise, while at higher harmonics the agreement between fitted and expected values is quite good. In a few cases the fitted value fluctuate below the expected value; in these cases the higher number is used in assigning an error to the results.

The situation is more complicated if a non-zero mean actually exists, which is the case of interest. While the real and imaginary parts distribute normally about a point not at the origin, the marginal distributions in the norm and phase are quite complicated. These are discussed in detail in Appendix A, together with some difficulties which inevitably occur. We quote errors in two ways: The

1.52σ circle about the point in the complex plain encloses the right answer with 68% probability, so it is analogous to a 1σ error in one variable. We also quote asymmetric errors on the norms, choosing them in such a way that the area of the distribution from the norm to the upper (or lower) bound is 34%, again in analogy to the usual normal distribution. The important caveat is that the most probable result is greater than the true result. In the case of a Rayleigh distribution, where the true norm is zero, the most probable result is σ.

V. ANISOTROPY RESULTS

a) Sidereal harmonics

The Fourier amplitude spectrum for the combined data (1978 January through 1983 May) in the region near 1 day^{-1} is shown in Fig. 2. Peaks at the solar and sidereal frequencies (1.000 day^{-1} and 1.027 day^{-1}) are clearly visible. If a real effect at the solar frequency is modulated at an annual frequency, then sidelobes of the same size should appear at the sidereal frequency, $(1 + 1/365)$ day^{-1}, and the "antisidereal frequency," $(1 - 1/365)$ day^{-1}. The absence of a peak at the antisidereal frequency may be taken as evidence that such modulation is not occurring, and that the signal at the sidereal frequency is real.

It is of course not difficult to find other peaks of similar size elsewhere in the data, as is evident from the noise distribution shown in the Appendix. The claim that the sidereal peak is real is based upon its occurrence at a frequency of *a priori* interest and the stability of its amplitude and phase with time. The same can be said of the solar peak, although here the claim is less secure because of the smaller signal.

Further details at the sidereal first harmonic frequency are shown in Table 1. Primed variables represent "raw" quantities, uncorrected for solar motion or detector latitude. The phase and amplitude, ξ_1 and α_1, have been corrected for solar motion relative to the LISM assuming a solar velocity of 21.6 km s^{-1} (Adams and Frisch 1977) toward $\alpha_I = 16^{\rm h}.8$ and $\delta_I = -15°$ (Weller and Meyer 1974). Because of a complete reanalysis, the results for the first half of the data are slightly

different that those reported in CBDG.

Figure 3 shows the raw norms and phases on the conventional "harmonic dial" plot. The circles are at 1.52 σ, as discussed above, and should contain the actual norm with 68% probability.

We conclude that a signal at the sidereal frequency has been observed at the 99% confidence level.

The Fourier amplitude spectrum near twice the solar frequency is shown in Fig. 4, and the spectrum in the vicinity of three times the solar frequency in Fig. 5. In both cases a sidereal peak can be seen, and no solar effect is evident. Table 2 summarizes the data at the sidereal second harmonic. Results for the first five sidereal harmonics are summarized in Table 3. It is highly probable that a third harmonic exists, but no higher harmonics can be seen.

The phases of the second and higher harmonics have been chosen as the smallest positive possibilities, and all the amplitudes have been taken as positive. In accord with the earlier discussion, we should expect the phase of the mth harmonic to differ from that of the first by 0 or π/m, depending upon the sign of of the mth amplitude in equation (2.2). It is evident from Table 3 that the phase agreement between the first and second harmonics is consistent if the sign of ξ_2 is negative, corresponding to outflow at the poles and inflow in the equatorial plane. But what about the third harmonic?

Since the real and imaginary parts of the Fourier amplitude A_m at the mth sidereal harmonic distribute normally, it is easily demonstrated that the best estimator of ξ_m at an arbitrary right ascension α (in hours) is given by

$$\xi_m^* = \mathrm{Re}(A_m)\cos m(2\pi/24)\alpha + \mathrm{Im}(A_m)\sin m(2\pi/24)\alpha \ . \qquad (5.1)$$

The contribution of the mth harmonic to χ^2 is then given by

$$\frac{\left(\xi_m^*\cos m(2\pi/24)\alpha - \mathrm{Re}(A_m)\right)^2}{\sigma_m^2} + \frac{\left(\xi_m^*\sin m(2\pi/24)\alpha - \mathrm{Im}(A_m)\right)^2}{\sigma_m^2} \ . \qquad (5.2)$$

The contributions for the first five harmonics to the overall χ^2 are shown in Fig. 6, as is the contribution from an uncorrected first harmonic. As expected from the above discussion, a symmetry axis at about $2^h.8$ yields a good fit for the first and second harmonics. However, any overall fit including the first, second, and third harmonics produces an unacceptable χ^2. The inconsistency is between the phases of the second and third harmonics; the first harmonic could accommodate either but not both.

A final way to look at the data is shown by the "folded light curve" in Fig. 7. In this case the data were simply added, folding at the sidereal period, to obtain the plotted points. The data in Fig. 7(a) are uncorrected for LISM motion; the first harmonic correction for this motion is shown by the dashed sine wave. In Fig. 7(b) the correction has been added to the data. In both cases the solid curves are drawn using the amplitudes and phases given in the tables for the first three harmonics. Although the two-hour binning limits resolution to the point spacing, it is evident that harmonics higher than the third are not needed to describe the data.

b) Solar harmonics

Figure 8 shows a similar folded light curve at the solar frequency. The solid curve is the *a priori* expectation due to the motion of the earth around the sun, according to Eq. 2.6, and the dot-dashed curve is a two-parameter least squares fit. While the probability of no effect is about 8%, it is interesting that the effect predicted by Compton and Getting in 1934 seems to be observed, possibly for the first time. A more complete discussion of this analysis is given elsewhere (Cutler and Groom 1986).

c) Meterological Effects

The observed muons are the decay products of mesons produced in the cascades initiated by primary protons or heavier nuclei. As a result, the intensity is sensitive to the balance between meson decay and subsequent hadronic interaction. If the temperature near the production height increases, the air becomes more rarified

and the muon intensity increases. The expected fractional intensity coefficient is $29 \times 10^{-4}/°C$. An increase in barometric pressure at the surface means more material between the production point and detector, and hence there is a small negative pressure coefficient. The observed pressure coefficient reported by various groups is considerably larger, and in CBDG we pointed out that this was apparently due to the correlation between surface pressure and high-altitude temperature.

During the early years of operation, we monitored radiosonde temperature/ pressure profiles obtained from balloon flights made every 12 hours from the Salt Lake City international data. Because of large instrumental setting errors, these data were of limited value. As discussed in CBDG, we concluded that (a) stratospheric temperature variations are very small, and that (b) the large pressure coefficient found by other groups is very likely a consequence of the correlation between surface pressure and high-altitude temperature. At frequencies below 1 day^{-1}, our Fourier amplitudes are dominated by a noise spectrum consistent with $1/f$, which we interpret as a consequence of pressure and temperature effects. However, the data smoothing apparently removes these effects at frequencies of interest. As has been discussed above, the measured variance (as obtained from the noise at nearby frequencies) is somewhat larger than the expected variance (from the total number of counts), particularly at the first and second harmonics, and we interpret this as the residual effect of temperature and pressure variations.

d) Comparison with Other Experiments

Since the publication of CBDG, new results have been reported by the Poatina (Humble, Fenton, and Fenton 1987) and Mt. Norikura (Nagashima *et al.* 1989) groups. In addition, there are now results from Baksan (Andreyev *et al.* 1987), Hong Kong (Lee and Ng 1987), and Matsushiro (Mori *et al.* 1987).

It is not appropriate to present a critical review of these rather different experiments here. Data have been selected, analyzed, presented, and interpreted in different ways by different groups. In no case was it demonstrated that the reported sidereal amplitude peaked at the sidereal frequency, and errors were assigned in

different and occasionally questionable ways. In only one case (Lee and Ng 1987) were the data corrected for solar motion with respect to the LISM. To compare the results in Fig. 9, we have taken the amplitude and error at face value, corrected for solar motion, and divided by the cosine of the effective latitude of the station.

The limited data available in 1981 were consistent with a single value which was independent of median rigidity (or energy). Many of the new data points shown in Fig. 9 are higher, and the consistency is gone. The new Norikura point is consistent with the old measurement. The Poatina point is also consistent with the old measurement, but has increased so that it is now substantially above the Holborn and Utah results. It is difficult to understand the Matsushiro and Baksan points, unless the anisotropy has somehow increased in the last decade.

There is reasonable agreement as to the phase of the first harmonic. Several groups report a second harmonic, and again the agreement between them is reasonable.

In the earlier analysis, unsuccessful attempts were made to extract some declination information by combining the Poatina first-harmonic data with the Utah first- and second-harmonic data. The situation has not improved.

VI. CYGNUS X-3 SEARCH

a) Raw signal

Correlation between 4.8 hour X-ray emissions from Cygnus X-3 and cosmic-ray muon flux variations has been reported in data from the Soudan (Marchak *et al.* 1985) and NUSEX (Battistoni *et al.* 1985) detectors. The Soudan detector recorded data between September 1981 and November 1983, with a 0.96 year live time. The signal was not observed in later experiments (Cherry 1986, Dingus *et al.* 1988). However, radio and optical emission from this object show dramatic time variations, and it has been argued that whatever was seen by these detectors was not present at a later time (Cherry 1986). It was therefore particularly interesting to reanalyze the Utah data to search for a signal in the relevant frequency range,

since data were obtained during the same time interval.

For technical reasons, 2-hour binning was used for the analysis reported in the previous sections, even though data were recorded with 0.5-hour binning. To search at frequencies near 1/(4.8 hr), the data were rebinned into uniformly spaced half-hour bins. They were then conditioned and Fourier analyzed as described above, with one important exception. In the anisotropy analysis, data from sectors of the detector pointing to different parts of the sky were rebinned with phasing corresponding to the appropriate hour angles. In this case, different sectors observe Cygnus at different times, and the data were combined after correction for both the time and the corresponding Cygnus phase differences. The resulting DFT near 0.2 day^{-1} is shown in Fig. 10. There is in fact a marginal signal at the Cygnus X-3 frequency (5.0079376/solar day, or 4.9943/sidereal day), with amplitude $(1.5^{+0.8}_{-0.5}) \times 10^{-4}$). The radius of the 68% confidence circle (1.52σ) is 1.1×10^{-4}. The phase of the DFT is such that a maximum occurred at 2.1 ± 0.5 h UT on 1 Jan 1978, corresponding to a phase of 0.65 ± 0.10 with respect to the time of the x-ray minimum. The period and phase are those given by van der Klis and Bonnet-Bidaud (1981).

Fig. 11 shows the result of folding the data with a period of 0.1996830 days. A least squares fit to a sine wave gives an amplitude $(1.7^{+0.8}_{-0.5}) \times 10^{-4}$ with a maximum occurring at 2.2 ± 0.5 h UT on 1 Jan 1978, or a phase of 0.67 ± 0.10. The standard deviation for each point is 1.3×10^{-4} and χ^2 for the fit is 4.8 with 5 degrees of freedom. For no effect, χ^2 is 10.7 with 7 degrees of freedom. The slight differences in amplitude and phase between this fit and the DFT are the result of the somewhat different ways missing data are treated by the algorithms.

b) Attempts at enhancement

A window at the sidereal period centered on the right ascension of Cygnus X-3 should increase the signal in inverse proportion to the width of the window, as long as the window is wider than the detector response width. Random noise will increase in inverse proportion to the square root of the width of the window. Con-

sequently, the signal-to-noise ratio should be inversely proportional to the square root of the window width. A high-pass filter must be applied to the data before windowing to prevent spurious signals at the Cygnus X-3 frequency resulting from the product of the sidereal window with low-frequency components of the data.

Fits of this sort were made using 12-hour and 6-hour windows, with a 12-hour running average subtracted from the data in constructing the $x(n\Delta t)$. The high-pass filter produced a slight decrease in the amplitude of the signal in the unwindowed case as compared with that shown in Fig. 11. The amplitude increased as expected when the windows were applied, but the signal/noise ratio showed no noticeable improvement.

Fits were also made with the window centered at different right ascensions. This signal appeared to be greater when the detector is pointing towards Cygnus than when it is pointing away.

These experiments are analogous to position cuts in the data from other detectors. Since no signal enhancement could be produced using the Mayflower data, we conclude that better position information would not help. Indeed, the beat phenomenon between the data window (position-cut data) and the low-frequency noise present in any unfiltered real data (but usually not Monte Carlo data) can easily produce spurious signals in any analysis.

c) Beat frequencies

Because a given sector of the detector observes Cygnus X-3 for only a small fraction of a day, much of the amplitude information about the signal will be contained in side-lobe harmonics resulting from the beating of the Cygnus frequency with the harmonics of the detector response. The amplitude and phase observed at each of these beat frequencies will be an independent measurement of the Cygnus X-3 signal, and the appropriate average of the complex amplitudes provides our best estimate of the signal. In particular, the sensitivity of the detector to a source

which is overhead at time t_0 can be written as

$$D(t) = a_0 + \sum_{n=1}^{\infty} a_n \cos n\omega_\star (t - t_0) \tag{6.1}$$

where the a_n's are the Fourier amplitudes of the detector response, and $\omega_\star$ is the sidereal frequency. The a_n's are readily calculated, and, because of the sharp response, they decrease very slowly with n. Similarly, a possible periodic signal associated with Cyg X-3 can be represented by

$$Cy(t) = b_0 + \sum_{m=1}^{\infty} b_m \cos m\omega_X (t - t_X) \tag{6.2}$$

where b_n is the Fourier amplitude of its nth harmonic, ω_X is its frequency, and it reaches its maximum at time t_X. The x-ray curve for Cyg X-1 is dominated by a first harmonic, so for our present purposes we keep only the first term in the series. The observed signal will be the product of the Cygnus signal and the detector response:

$$\begin{aligned} D(t)Cy(t) = b_0 a_0 &+ \sum_{n=1}^{\infty} b_0 a_n \cos \omega_\star (t - t_0) \\ &+ b_1 a_0 \cos(\omega_X t - \phi_0) \\ &+ \frac{1}{2} \sum_{n=1}^{\infty} b_1 a_n \cos(\omega_n t - \phi_n) \\ &+ \frac{1}{2} \sum_{n=-1}^{-\infty} b_1 a_n \cos(\omega_n t - \phi_n) \end{aligned} \tag{6.3}$$

where $\omega_n = \omega_X + n\omega_\star$, and $\phi_n = \omega_X t_X + n\omega_\star t_0$. Note that

a) the signal from Cygnus contributes to all of the sidereal harmonics;

b) the first harmonic discussed in section (a) above has amplitude $b_0 a_0$;

c) since $a_n \approx a_0$ for the values of n under consideration, signals should show up at many observable harmonics, with predictable relative phases, and amplitudes equal to nearly half that of the first harmonic.

Results of this analysis are given in Fig. 12. For $n \neq 0$ we have plotted $2a_0/a_n$ times the Fourier amplitude, so that any real signals should be the same in all channels.

Since the real and imaginary parts of the DFT independently distribute normally, the results are readily combined to yield an amplitude 0.8×10^{-4}. The standard deviation is 0.4×10^{-4}, so with 68% probability the signal is within a radius of 0.6×10^{-4}. The χ^2 for the combined real and imaginary parts is 15.2 with 16 degrees of freedom. For a no-effect hypothesis, $\chi^2 = 19.4$ with 18 degrees of freedom. If the effect were bidirectional (*e.g.* induced by neutrinos) then a larger effect would be seen at the harmonics with even n, *i.e.* at multiples of twice per sidereal day. Nothing of significance is seen. These and other results are summarized in Table 4.

The second harmonic of the Cygnus X-3 signal has an amplitude $(0.5^{+0.5}_{-0.1}) \times 10^{-4}$ with maxima at phases 0.71 ± 0.14 and 0.21 ± 0.14. The standard deviation of the combined real or imaginary parts is 0.41×10^{-4}. For no effect, χ^2 is 15.1 with 18 degrees of freedom and the χ^2 for the fit is 13.8 with 16 degrees of freedom.

d) Conclusions

The Mayflower data show a weak signal at the Cyg X-3 frequency with the same phase as that observed at Soudan and NUSEX. It is not substantially strengthened by windowing, and the expected confirmation at other harmonics is absent.

There is no reason to expect the energy spectrum of the muons expected to come "from Cygnus" to be the same as that from the decay of secondary mesons in the atmosphere. If it is, the average fraction of the time the Mayflower Mine detector observes Cygnus is 0.034. From this fraction, the detector aperture, and the rates reported in CBDG, we obtain a flux of $2.2 \times 10^{-8} \mathrm{cm}^{-2}\mathrm{s}^{-1}$ "from Cygnus" at a depth where the muon threshold energy is 130 GeV. The error is $1.4 \times 10^{-8} \mathrm{cm}^{-2}\mathrm{s}^{-1}$ *if* the phase is constrained to its best fit value. The vertical muon flux for normal cosmic ray muons at the Mayflower Mine detector is 45 times larger than that at Soudan. Again with the assumption that the Cygnus-associated muons have the

same spectrum, our sensitivity is thus about 7 times less than at Soudan.

VII. CONCLUSIONS AND DISCUSSION

The firmest conclusion from the experiment is the same as that stated in CBDG: at a rigidity large enough so that the effects of the solar wind and other manifestations of the solar magnetic field are small, the cosmic ray flux is remarkably isotropic. The uncorrected first harmonic at the latitude of the Utah detector is less than 0.04% at the 90% confidence level. It is always possible that this is just the result of an accidental alignment of the streaming direction and the Earth's axis, but $|\cos\delta| > 0.5$ for 87% of the sky, and a 0.1% anisotropy is still quite small. Such a stagnant cosmic ray plasma is incompatible with the spallation product abundance data if the cosmic rays spend their entire lifetime in the disk, but consistent with the longer lifetime inferred from the $^{10}Be/^{9}Be$ measurements. The cosmic rays we observe have spent perhaps 90% of their lifetime outside the disk while remaining trapped in the galaxy's magnetic fields.

Three temporal harmonics have been observed at confidence levels which have significantly improved since CBDG. The phase of the first is in agreement with world data, although we measure a smaller amplitude than is obtained by several other groups. If there is a symmetry axis (the streaming direction) then the relative phase of the temporal harmonics is determined. This can be done for our first and second or our first and third harmonics, but not for all three.

Analysis at the Cygnus X-3 $(4.8\ \mathrm{hr})^{-1}$ frequency shows a weak signal which is not robust under various attempts at enhancement. The observation period overlapped that of the Soudan detector. However, if the presumed Cygnus "muon spectrum" is similar to the normal muon spectrum (from the decay of secondary mesons in the atmosphere), then our sensitivity is less that that of the Soudan detector by a factor of seven.

A number of experimental lessons were also learned. The most serious of these concerned the importance of clean, dependable power. We did not anticipate the

removal of the electric substation when the mine closed, and economic considerations forced the use of power from an unregulated transformer used mainly to power substation switches. The on-line computer and tape deck used in the experiment were particularly vulnerable to turn-on transients and other variations in the unconditioned power. Almost all of the down time, as well as computer and tape deck failures, were due to these problems. In retrospect, investment in non-interrruptable power supplies at the outset would have resulted in a much better experiment.

Phototubes were glued to light guides using optical epoxy. The thermal shock of moving the counters from campus to the mine weakened or broke many of the joints, many of which were repaired at the time of installation. However, continued joint deterioration during the lifetime of the experiment resulted in a degradation of performance. High voltages were originally set so that all pulse heights were safely above discriminator thresholds, but near the end of the experiment rates were decreasing at about 2% per year. A dual discrimination system was supposed to have permitted early detection of such effects, but the software was not properly implemented. In practice the deterioration did not affect the analysis, because the signal was measured relative to a running average.

This work was supported, in part, by NSF grants AST80-10727 and PHY83-08135. Publication at Lawrence Berkeley Laboratory was supported by D.O.E. Contract No. DE-AC03-76SF00098. The experiment, at a remote location in the Wasatch Mountains, and without wintertime road access, was kept running through several difficult winters only by the dedicated efforts of H. A. Horton. Discussions about the unpleasant properties of the off-center Rayleigh distribution with G. R. Lynch and O. Dahl were invaluable.

APPENDIX A

OFF-CENTER RAYLEIGH DISTRIBUTIONS

I. DISTRIBUTION OF REAL AND IMAGINARY PARTS

In an experiment like that described in this paper, the probability that a count occurring in a short time dt is proportional to dt. The number of counts observed in a finite interval Δt is therefore chosen from a Poisson distribution with mean value λ. Because a real signal may be present at one or more frequencies, λ may vary from interval to interval. We assume that the data string includes a large number of cycles at any frequency of interest, and that the total number of counts in the data string is large.

We wish to obtain the probability density functions (p.d.f.'s) for the real and imaginary parts (ζ and η) of the one-sided discrete Fourier amplitude (DFT) given by

$$\zeta_k + i\eta_k = \frac{2}{\mathcal{N}} \sum_{n=0}^{N-1} m_n \, e^{-i\theta_{kn}} \ , \qquad (A1)$$

where

$\mathcal{N}$ = total number of events in the data string

N = total number of intervals of length Δt

m_n = number of counts in the nth interval

$\theta_{kn} = 2\pi f_k n \, \Delta t$

f_k = the frequency of interest, taken to be less than $1/\Delta t$.

(Equation (A1) is a somewhat idealized version of equation (4.2).) We may assume that signals exist in the transformed data at discrete frequencies f_ℓ; these have amplitudes $\zeta_{0\ell} + i\eta_{0\ell}$. Then the mean number of counts in the nth interval is given by

$$\lambda_n = \frac{\mathcal{N}}{N}\Big\{1 + \sum_\ell \zeta_{0\ell} \cos\theta_{\ell n} + \sum_\ell \eta_{0\ell} \sin\theta_{\ell n}\Big\} \ , \qquad (A2)$$

where we have approximated the expected (large) total number of counts by the observed number.

It is convenient to deal with characteristic functions (c.f.'s) rather than the p.d.f.'s themselves, where the c.f. $\phi(u)$ associated with the p.d.f. $f(x)$ is given by

$$\phi(u) \equiv E(e^{iux}) = \int_{-\infty}^{\infty} f(x)\, e^{iux} dx \qquad (A3)$$

(Cramér, 1958). The c.f. for a Poisson distribution with mean λ is $\exp\{\lambda(e^{iu} - 1)\}$, while that for a Gaussian distribution with mean x_0 and standard deviation (s.d.) σ is $\exp(iux_0 - \frac{1}{2}\sigma^2 u^2)$. If x has p.d.f. $f_1(x)$ and c.f. $\phi_1(u)$ and y has p.d.f. $f_2(y)$ and c.f. $\phi_2(u)$, then the c.f. of the weighted sum $ax + by$ is given by $\phi_1(au)\phi_2(bu)$. Since m_n is chosen from a Poisson distribution, it then follows from these considerations and equation (A1) that the c.f. corresponding to the p.d.f. of ζ_k is given by

$$\phi(u) = \prod_{n=0}^{N-1} \exp\left\{\lambda(e^{i(2/\mathcal{N})u\cos\theta_{kn}} - 1)\right\} . \qquad (A4)$$

Expanding the complex exponential and inserting λ_n from equation (A2), we obtain

$$\begin{aligned} \phi(u) = \exp\Bigg\{ \sum_m \frac{\mathcal{N}}{N}\Bigg(1 + \sum_\ell \zeta_{0\ell}\cos\theta_{\ell n} + \sum_\ell \eta_{0\ell}\sin\theta_{\ell n}\Bigg) \\ \times \left(i\frac{2u}{\mathcal{N}}\cos\theta_{kn} - \frac{1}{2}\frac{4u^2}{\mathcal{N}^2}\cos^2\theta_{kn} + \ldots\right)\Bigg\} . \end{aligned} \qquad (A5)$$

Since the number of cycles is large, the only nonvanishing terms in the summation over n are $\sum \cos\theta_{\ell n}\cos\theta_{kn} = (N/2)\delta_{k\ell}$, so that

$$\phi(u) = \exp\left\{iu\zeta_{0k} - \tfrac{1}{2}(2/\mathcal{N})u^2 + \ldots\right\} .$$

$\phi(u)$ is very small unless $2u^2/\mathcal{N} \lesssim 1$, so terms of higher order in $2u/\mathcal{N}$ may be neglected in regions where $\phi(u)$ is substantially nonzero. We recognize $\phi(u)$ as the c.f. of a Gaussian p.d.f. with mean $\zeta_{0\ell}$ and s.d. $\sqrt{2/\mathcal{N}}$. An analogous calculation for the imaginary part of the DFT yields a Gaussian with mean $\eta_{0\ell}$ and the same standard deviation. We conclude that subject only to the conditions stated at the beginning of this section, the real and imaginary parts of the DFT independently distribute normally about their true values with s.d. $\sqrt{2/\mathcal{N}}$.

II. DISTRIBUTION IN ANGLE AND PHASE

The general picture is shown in Figure 13. The probability is represented by a Gaussian peak centered at the Fourier amplitude $\zeta_0 + i\eta_0$ at a given frequency (we henceforth suppress the frequency index). Given the true mean at $\zeta_0 + i\eta_0 = \xi_0 \exp(i\theta_0)$, the probability of obtaining amplitude and phase (ξ, θ) is simply the product of the two Gaussian marginal distributions in ζ and η. Since $d\zeta\, d\eta = \xi\, d\xi\, d\theta$, this may be rewritten as

$$f(\xi, \theta|\xi_0, \theta_0)\xi\, d\xi\, d\theta = \frac{1}{2\pi\sigma^2} e^{-\rho^2/2\sigma^2} \xi\, d\xi\, d\theta\ , \qquad (A6)$$

where $\rho^2 = \xi^2 - 2\xi\xi_0 \cos\phi + \xi_0^2$, and $\phi = \theta_0 - \theta$. For example, if $\xi_0 = 0$ we obtain the familiar Rayleigh distribution for the marginal distribution in ξ:

$$g(\xi|\xi_0 = 0) = \frac{1}{\sigma^2}\xi\, e^{\xi^2/2\sigma^2} = \frac{d}{d\xi} e^{\xi^2/2\sigma^2} \qquad (A7)$$

Since no signal should appear at most frequencies, this p.d.f. should describe our DFT amplitude distribution at frequencies sufficiently high that white noise dominates. The distribution of amplitudes at 7000 frequencies above 0.7 day^{-1} is shown in Figure 14. The solid curve is of the form given in Equation (A7), with σ adjusted for a best fit. The fitted and expected ($\sqrt{2/\mathcal{N}}$) standard deviations are shown by the dashed and dotted lines, respectively.

In general, the marginal distributions in ξ and θ are given by

$$g(\xi|\xi_0) = \int f(\xi, \theta|\xi_0, \theta_0)\xi d\theta \qquad (A8)$$

$$h(\theta|\theta_0) = \int f(\xi, \theta|\xi_0, \theta_0)\xi d\xi \qquad (A9)$$

where we have chosen to define $g(\xi|\xi_0)$ so that $g(\xi|\xi_0)d\xi$ is the probability of an occurrence in the interval $d\xi$. With the definitions $\phi = \theta_0 - \theta$, $y = \xi/\sigma$, and

$y_0 = \xi_0/\sigma$, and with the help of Equation 8.431.3 in Gradshteyn and Ryzhik (1965), the integrals become

$$g(y|y_0) = y\, e^{-(y_0^2+y^2)/2} I_0(y_0 y) \qquad (A10)$$

$$h(\theta|\theta_0) = \frac{1}{2\pi} e^{-y_0^2/2} + \frac{w}{\pi} e^{-y_0^2 \sin^2\phi/2} \int_{-w}^{\infty} e^{-x^2} dx \qquad (A11)$$

where I_0 is a modified Bessel function and $w = (y_0/\sqrt{2})\cos\phi$. For large y_0, i.e. for $\xi_0 >> \sigma$, Equation (A11) simplifies to

$$h(\theta|\theta_0)\, d\theta \approx \frac{y_0}{\sqrt{2\pi}} e^{-y_0^2 \sin^2\theta/2} d(\sin\theta) \ .$$

The function is thus asymptotically Gaussian in $\sin\theta$, as might have been anticipated from Figure 13.

These functions have been tabulated for purposes of calculating the errors and confidence limits given in the main text.

III. INVERSION OF THE DISTRIBUTIONS

Equations (A6), (A10), and (A11) describe the distributions obtained by an ensemble of experiments if the true means ξ_0 and θ_0 are given. The experimental problem is just the opposite: if results ξ and θ are obtained in a single experiment, what can be said about the means and distributions of the true results ξ_0 and θ_0? We need $f(\xi_0, \theta_0|\xi, \theta)$ rather than $f(\xi, \theta|\xi_0, \theta_0)$. The connection is provided by Bayes' theorem, which for our purposes states that

$$F(\xi_0, \theta_0|\xi, \theta) = \frac{\psi_0(\xi_0, \theta_0)}{\psi(\xi, \theta)} f(\xi, \theta|\xi_0, \theta_0) \ , \qquad (A12)$$

where ψ and ψ_0 are the marginal p.d.f.'s for (ξ, ψ) and (ξ_0, ψ_0), respectively. For example,

$$\psi(\xi, \theta) = \int f(\xi, \theta|\xi_0, \theta_0)\psi_0(\xi_0, \theta_0)\, \xi_0 d\xi_0 d\theta_0 \ . \qquad (A13)$$

In the absence of any theoretical input whatsoever, we assert that the point (ξ_0, θ_0) might fall anywhere in the complex plane with equal probability, so that

ψ_0 is a constant. In this case equation (A13) states that $\psi(\xi, \theta)$ is equal to the same constant, and equation (A12) becomes

$$F(\xi_0, \theta_0 | \xi, \theta) = f(\xi, \theta | \xi_0, \theta_0) \; . \qquad (A14)$$

Similarly, the inversions of the two marginal distributions given by equations (A8) and (A9) are

$$G(\xi_0 | \xi) = g(\xi | \xi_0) \qquad (A14)$$

$$H(\theta_0 | \theta) = h(\theta | \theta_0) \; . \qquad (A15)$$

The same results can be obtained in a more heuristic manner. We obtain the real and imaginary parts ζ and η in the experiment, and each is the best estimator of ζ_0 and η_0. The true value ζ_0 (or η_0) distributes normally about ζ (or η), and the joint distribution is the product of the two marginal distribution. An equal-probability contour is shown by the dotted line in figure 13. We have simply reversed variables, and so of necessity $F(\xi_0, \theta_0 | \xi, \theta) = f(\xi, \theta | \xi_0, \theta_0)$.

This problem has also been treated by Linsley (1975), with a different result. His form may be obtained if it is assumed that the *a priori* distribution ψ_0 is proportional to $1/\xi_0$.

IV. PITFALLS

Although ζ and η are independent variables, ξ and θ are highly correlated, which contributes a certain amount of deception and confusion to the treatment of anisotropy results. For example, from equation (A10) it may be seen that the most probable result $\xi = \sigma y$ is obtained by solving

$$y_0 \, y \, \frac{I_1(y_0 y)}{I_0(y_0 y)} = y^2 - 1 \; ,$$

so that in general $\xi > \xi_0$. (If $y_0 = 2.838$, then the most probable y is 3.000.) The opposite result may be obtained from the inverted distribution. The problem

is intrinsic to the polar coordinate representation, and should be avoided by considering limits in the two-dimensional "harmonic dial" plot (figure ??) directly. Unfortunately, the "answer" in an anisotropy experiment is the radius vector ξ. In Tables I and II we have quoted errors corresponding to 68% confidence limits on ξ on the basis of equation (A10), but we have also have quoted the radii of circles which enclose the point (ξ_0, θ_0) with 68% probability. Both correspond to 1 s.d. limits in the usual one-dimensional case.

Curiously, our "paradox" and the properties of $g(\xi_0|\xi)$ also lead to "Greisen's Theorem," which states that the reported result ξ decreases in size and significance as a given experiment accumulates more data. Most anisotropy experiments report positive but marginal results, with the more sensitive experiments reporting smaller results. Even if the real effect is zero, the above analysis indicates at least a $1\,\sigma$ result 61% of the time. As σ decreases, ξ approaches ξ_0 from above.

TABLE 1

RESULTS AT THE SIDEREAL FREQUENCY

Variable	1978	1979	1980	Subtotal [a] 1978-80	1981	1982	1983	Subtotal [b] 1981-83	Total 1978-83
Duty cycle	75%	60%	76%	75%	53%	58%	58%	55%	64%
Muon counts $\times 10^{-8}$ ..	1.06	0.84	1.05	2.70	0.71	0.76	0.31	2.02	4.73
$10^4\sigma_0(=\sqrt{2/N_t})$	1.37	1.54	1.38	0.86	1.68	1.62	2.54	0.98	0.65
$10^4\sigma_1$ [c]	1.6	2.0	1.1[d]	1.0	1.8	1.8	3.9	1.1	0.7
$10^4\xi_1'$	$4.3^{+1.9}_{-1.3}$	$3.5^{+2.4}_{-1.2}$	$5.4^{+1.2}_{-1.0}$ [d]	$4.1^{+1.1}_{-0.9}$	$2.0^{+2.3}_{-0.7}$	$2.5^{+2.3}_{-0.9}$	$10.1^{+4.6}_{-3.0}$	$2.6^{+1.3}_{-0.8}$	$3.2^{+0.8}_{-0.6}$
α_1' (h)	1.4±1.5	5.6±2.3	2.0±0.8 [d]	2.9±1.0	13.9±3.3	1.1±2.8	0.1±1.5	23.9±1.7	1.9±0.9
$10^4 \times 68\%$ confidence circle radius [e]	2.5	3.0	2.1[d]	1.5	2.7	2.7	6.0	1.7	1.1
Prob. of noise $\geq \xi_1'$ ...	3.2%	21%	0.002% [d]	0.02%	50%	37%	3.6%	6.3%	0.01%
$10^4\xi_1$	$6.2^{+1.9}_{-1.4}$	$5.9^{+2.3}_{-1.6}$	$7.4^{+1.2}_{-1.1}$ [d]	$6.3^{+1.1}_{-0.9}$	$1.7^{+2.4}_{-0.4}$	$4.4^{+2.1}_{-1.3}$	$11.2^{+4.5}_{-3.1}$	$4.1^{+1.2}_{-0.9}$	$5.3^{+0.8}_{-0.7}$
α_1 (h)	2.6±1.0	5.3±1.3	2.9±0.6 [d]	3.6±0.6	8.4±4.0	2.9±1.6	0.9±1.4	2.3±1.1	3.2±0.5

[a] Subtotal to 1980 Aug 31, the cutoff date for the CBDG paper.

[b] Subtotal from 1980 Sept 01 to 1983 May 20, when the experiment was completed.

[c] σ_1 is the standard deviation of the real (or imaginary) part of the DFT, as determined from the data in a region near the first harmonic.

[d] Since $\sigma_1 < \sigma_0$, σ_0 is used to calculate errors in this column.

[e] Radius 1.52 σ.

TABLE 2

RESULTS AT TWICE THE SIDEREAL FREQUENCY

Variable	1978	1979	1980	Subtotal [a] 1978-80	1981	1982	1983	Subtotal [b] 1981-83	Total 1978-83
$10^4\xi_2$	$3.9^{+1.7}_{-1.1}$	1.2[c]	$4.7^{+1.9}_{-1.3}$	$3.2^{+1.2}_{-0.8}$	$1.9^{+2.0}_{-0.6}$	$4.2^{+2.2}_{-1.3}$	$4.5^{+3.6}_{-1.6}$	$2.8^{+1.3}_{-0.9}$	$2.9^{+0.9}_{-0.7}$
$10^4\sigma_2$	1.5	2.0	1.7	1.0	1.7	1.9	2.9	1.2	0.8
α_2 (h)	7.4±1.6	(7.8)[d]	8.9±1.4	8.0±1.2	5.9±3.5	9.3±1.7	9.5±2.6	9.0±1.6	8.4±1.1
$10^4 \times$ 68% confidence circle radius	2.3	3.0	2.5	1.5	2.5	2.8	4.5	1.7	1.2
Prob. of noise $\geq \xi_2$ ...	5.4%	84%	1.8%	0.8%	52%	7.4%	31%	4.7%	0.2%

[a] Subtotal to 1980 Aug 31, the cutoff date for the CBDG paper.

[b] Subtotal from 1980 Sept 01 to 1983 May 20, when the experiment was completed.

[c] Formal errors not quoted for $\xi < \sigma$.

[d] Parentheses indicate indeterminate result because $\xi < \sigma$.

TABLE 3

AMPLITUDES AND PHASES AT THE SIDEREAL HARMONICS

Variable	m					
	$1'$[a]	1[b]	2	3	4	5
$10^4\xi_m$	$3.2^{+0.8}_{-0.6}$	$5.3^{+0.8}_{-0.7}$	$2.9^{+0.9}_{-0.7}$	$2.1^{+0.8}_{-0.6}$	$0.8^{+0.9}_{-0.3}$	$1.4^{+0.8}_{-0.5}$
$10^4\sigma_m$	0.73	0.73	0.77	0.68	0.68	0.68
α_m (h)	1.9±0.9	3.2±0.5	8.4±1.1	0.0±1.2	(5.7)[c]	3.9±1.9
$10^4 \times$ 68% confidence circle radius	1.1	1.1	1.2	1.0	1.0	1.0
Prob. of noise $\geq \xi_m$	0.01%	0.01%	0.2%	0.7%	48%	11%
$\alpha_m - \alpha_1'$ (°)	0	—	97±21	91±23	56±50	29±32
$\alpha_m - \alpha_1$ (°)	—	0	79±18	72±20	38±49	11±30

[a] Uncorrected for solar motion relative to the LISM; these are the primed variables from Table 1.

[b] Corrected for solar motion relative to the LISM; these are the unprimed variables from Table 1.

[c] Parentheses indicate indeterminate result because $\xi < \sigma$.

TABLE 4

SUMMARY OF RESULTS FOR CYGNUS X-3 SIGNAL

Method	Amplitude $\times 10^4$	Phase	68% confidence radius $\times 10^4$	Probability of result $\geq$ amp.
DFT at Cygnus X-3 first harmonic	1.47	0.65	1.1	0.11
DFT at Cygnus X-3 second harmonic ...	0.48	0.71(0.21)	1.1	0.64
Folded light curve	1.68	0.67	1.1	0.06
Combined DFTs with phases shifted	0.81	0.55	0.6	0.14
—Even harmonics...	0.89	0.55	0.8	0.24
—Odd harmonics ...	0.65	0.55	1.1	0.45

REFERENCES

Adams, T. F., and Frisch, P. C. 1977, *Ap. J.*, **212**, 300.

Andreyev, Yu. M., Chudakov, A. E., Kozyarivsky, V. A., Sidorenko, A. M., Tulupova, T. I., and Voevodsky, A. V. 1987, *Proc. 20th Internat. Cosmic Ray Conf.* (Moscow), **2**, 22.

Battistoni, G. *et al.* 1985, *Phys. Lett.*, **155B**, 465.

Cherry, M. L. 1986, *Proceedings of the 1986 Summer Study on the Physics of the Superconducting Supercollider*, ed. by R. Donaldson and J. Marx, Snowmass, CO (1986), 640.

Compton, A. H., and Getting, I. A. 1935, *Phys. Rev.*, **47**, 817.

Cramér, H. 1958, *Mathematical Methods of Statistics* (Princeton: Princeton University Press).

Cutler, D. J., Bergeson, H. E., Davis, J. F., and Groom, D. E. 1981, *Ap. J.*, **248**, 1166.

Cutler, D. J., and Groom, D. E. 1986, *Nature*, **322**, 434.

Cutler, D. J., and Groom, D. E. 1987, *Proc. of the XXII Int. Conf. on High Energy Phys.*, ed. S. C. Loken (Singapore: World Scientific), 1317.

Daniel, R. R., and Stevens, S. A. 1975, *Space Sci. Rev.*, **17**, 45.

Davies, S. T., Elliot, H., and Thambyahpillai, T. 1979, *Proc. 16th Internat. Cosmic Ray Conf.* (Kyoto), **4**, 211.

B. L. Dingus *et al.*, *Phys. Rev. Lett.*, **60**, 1785.

Fenton, A. G., and Fenton, K. B. 1975, *Proc. 14th Internat. Cosmic Ray Conf.* (Munich), **4**, 1482.

Fenton, A. G., and Fenton, K. B. 1976, *Proc. 2nd Int. Cosmic Ray Symp. Japan*, 313.

Gaisser, T. K. 1974, *J. Geophys. Res.*, **79**, 2281.

Gaisser, T. K. 1976, *Proc. 2nd Int. Cosmic Ray Symp. Japan*, 33.

Garcia-Munoz, M., Mason, G. M., and Simpson, J. A. 1977, *Ap. J.*, **217**, 859.

Gleeson, L. J., and Axford, W. I. 1968, *Ap. Space Sci.*, **2**, 431.

Gombosi, T. *et al.* 1975*a*, *Nature*, **255**, 687.

Gombosi, T. *et al.* 1975*b*, *Proc. 14th Internat. Cosmic Ray Conf.* (Munich), **2**, 586.

Gradshteyn, I. S., and Ryzhik, I. M. 1965, *Table of Integrals, Series, and Products*, 4th Edition (New York: Academic Press).

Groom, D. E., and Morrison, J. L. 1975, Univ. of Utah Internal Report UUCR-153 (unpublished).

Groom, D. E., Loh, E. C., Nelson, H. N., and Ritson, D. M. 1983, *Phys. Rev. Lett.*, **50**, 573.

Hagen, F. A., Fisher, A. J., and Ormes, J. F. 1977, *Ap. J.*, **212**, 262.

Humble, J. E., Fenton, A. G., and Fenton, K. B. 1985, *Proc. 19th Internat. Cosmic Ray Conf.* (La Jolla), **5**, 39.

Király, P., Kóta, J., Osborne, J. L., Stapley, N. R., and Wolfendale, A. W. 1979, *Riv. Nuovo Cimento*, **2**, No. 7.

van der Klis, M., and Bonnet-Bidaud, M. 1981, *Astron. Astrophys.*, **95**, L5.

Lee, Y. W., and Ng., L. K. 1987, *Proc. 20th Internat. Cosmic Ray Conf.* (Moscow), **2**, 18.

Linsley, J. 1975, *Phys. Rev. Lett.*, **34**, 1530.

Shapiro, M. M., ed. 1982, *Composition and Origin of Cosmic Rays*, NATO ASI series C, No. 107.

Marchak, M. L. *et al.* 1985, *Phys. Rev. Lett.*, **54**, 2079.

Mori, S., Sagisaka, S., Yasue, S., and Ichinose, M. 1987, *Proc. 20th Internat. Cosmic Ray Conf.* (Moscow), **4**, 160.

Murakami, K., *et al.* 1976, *Proc. 2nd Int. Cosmic Ray Symp. Japan*, 13.

Nagashima, K., Funimoti, K., Fujii, A., Ueno, H., and Kondo, I. 1972, *Rept. Ionos. Space Res. Japan*, **26**, 31-68.

Nagashima, K., Fujimoto, K., Sakaibara, S., Fujii, Z., Ueno, H., Morishita, I., and Murakami, K. 1989, *Nuovo Cimento*, **12C**, 695.

Sakakibara, S., Ueno, H., Fujimoto, K., Fujii, Z., Kondo, I., and Nagashima, K. 1979, *Proc. 16th Internat. Cosmic Ray Conf.* (Kyoto), **4**, 216.

Weller, C. S., and Meyer, R. R. 1974, *Ann. Rev. Astron. Ap.*, **12**, 71.

Wiedenbeck, M. E., and Greiner, D. E. 1980, *Ap. J. (Letters)*, **239**, L139.

DAN J. CUTLER: Spectrum Systems, N. 2721 Van Marter Dr. #3, Spokane WA 99206.

DONALD E. GROOM: Particle Data Group, LBL 50-308, Berkeley CA 94720.

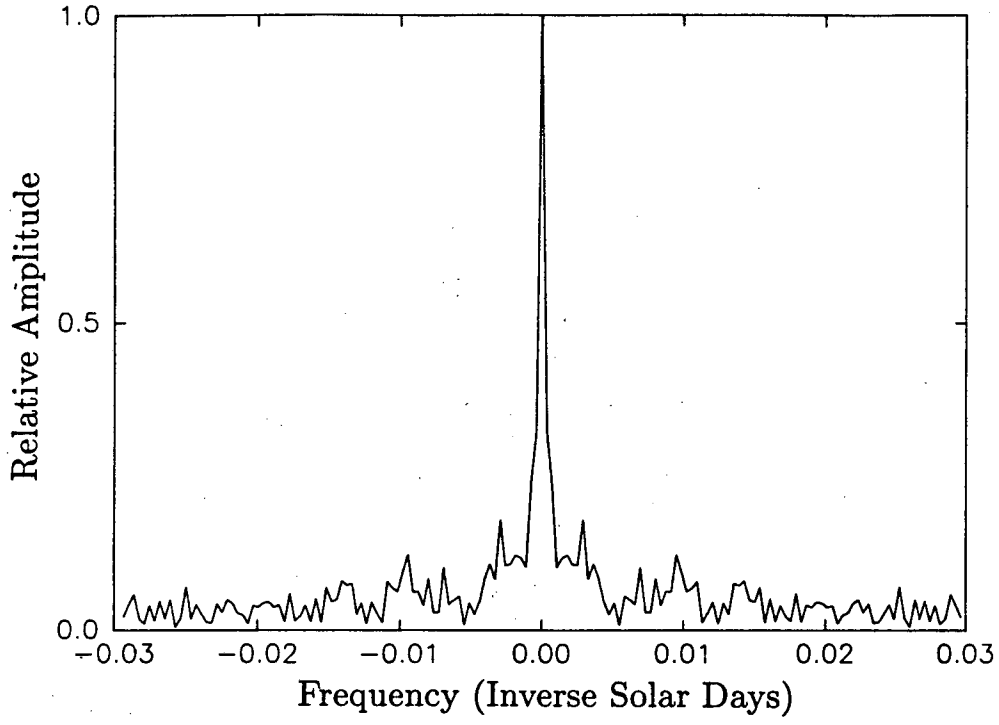

FIG. 1. Modulus of the Fourier transform for the data window for the entire experiment.

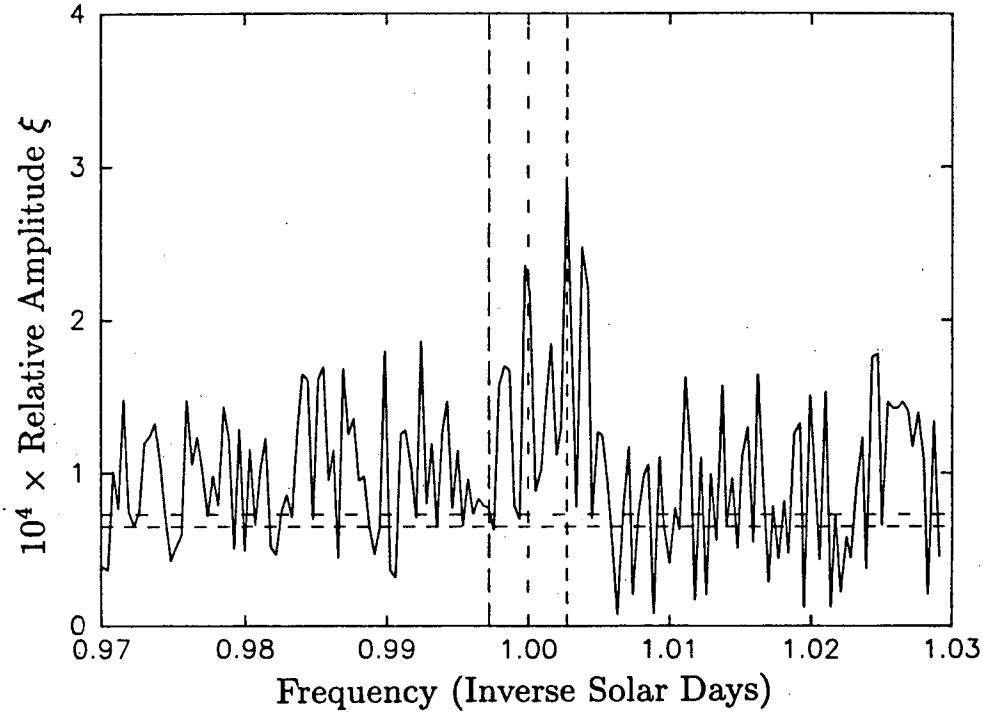

FIG. 2. DFT amplitude spectrum of the total data set near 1 day^{-1}. Vertical lines indicate the "antisidereal" frequency, solar frequency, and the sidereal frequency. The lower horizontal line indicates σ_0, and the higher one σ_1, as given in Table 1.

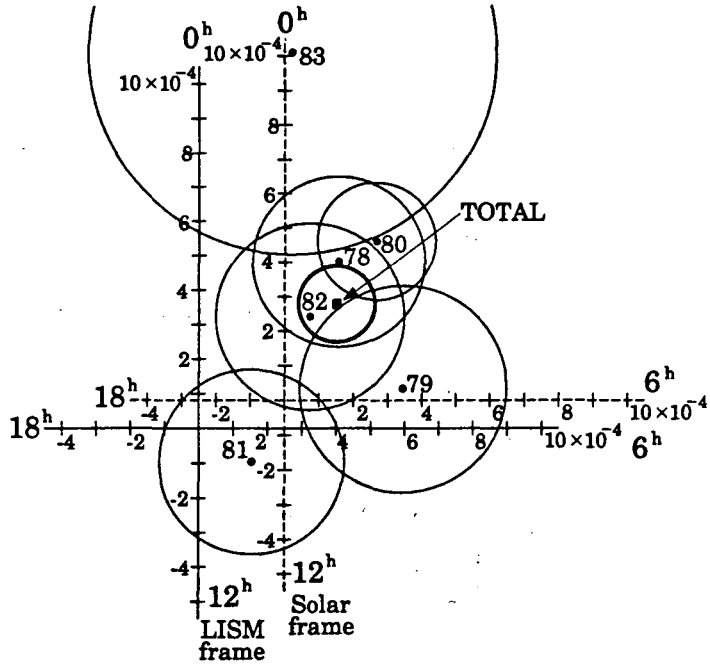

FIG. 3. Harmonic dial plot of first harmonics, as obtained from the annual and total data segments. The solid axes are with respect to the local interstellar medium, and the dotted axes are heliocentric.

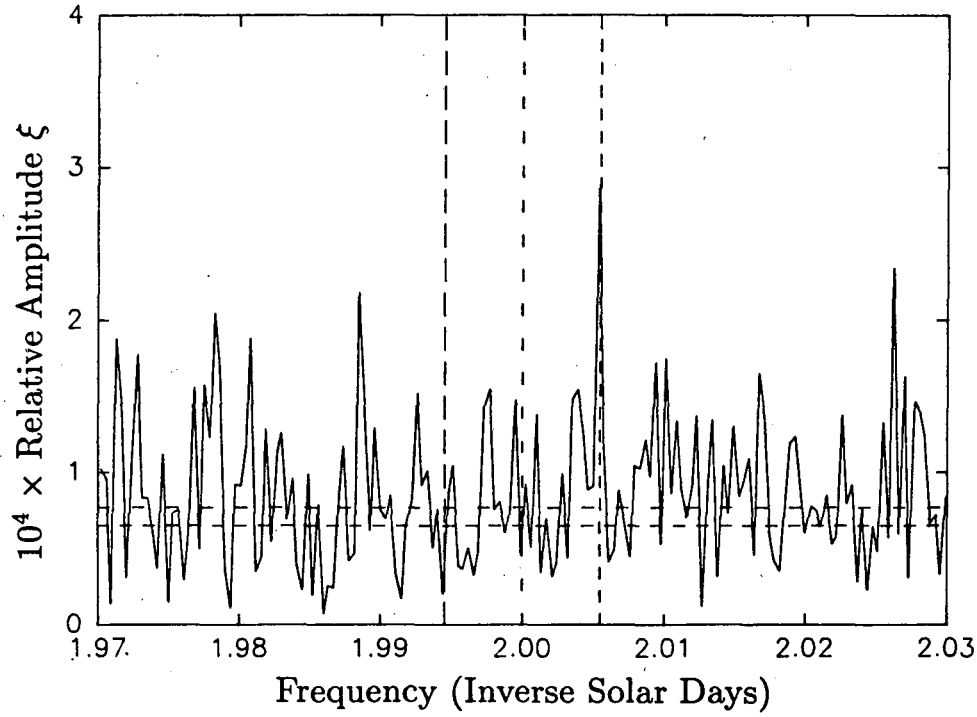

FIG. 4. DFT amplitude spectrum of the total data set near 2 day^{-1}. Vertical lines indicate twice the "antisidereal" frequency, solar frequency, and the sidereal frequency. The lower horizontal line indicates σ_0, and the higher one σ_2, as given in Table 2.

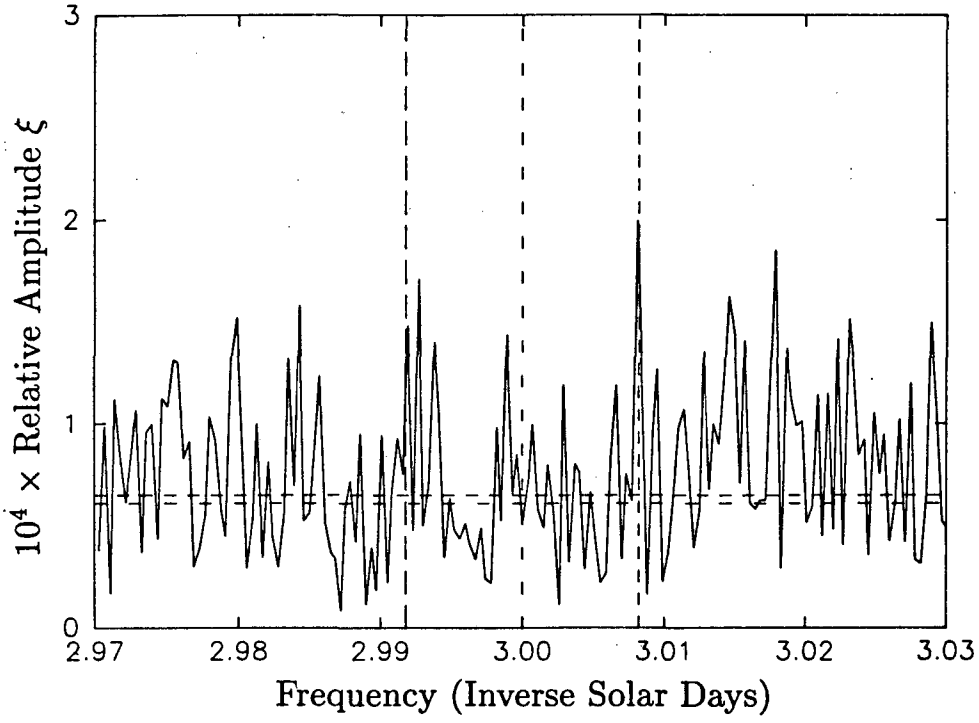

FIG. 5. DFT amplitude spectrum of the total data set near 3 day^{-1}. Vertical lines indicate twice the "antisidereal" frequency, solar frequency, and the sidereal frequency. The lower horizontal line indicates σ_0, and the higher one σ_3, as given in Table 3.

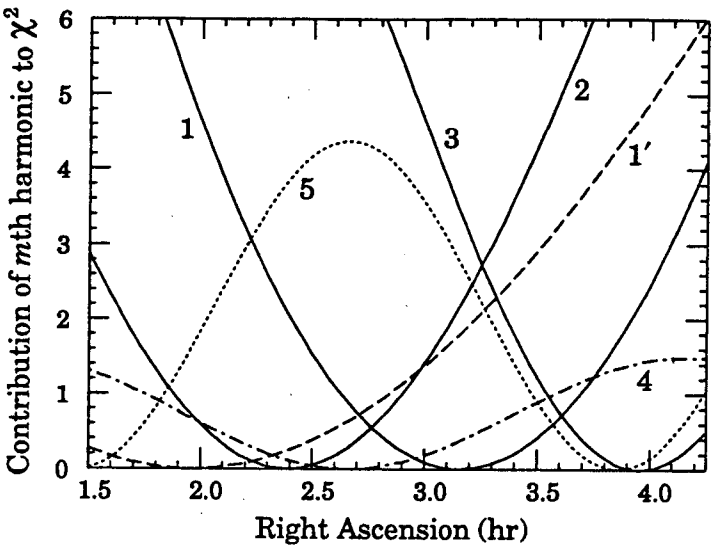

FIG. 6. Contribution of the five fitted harmonics to χ^2 at right ascension α. The uncorrected first harmonic contribution is also shown, as indicated by the curve labled 1′.

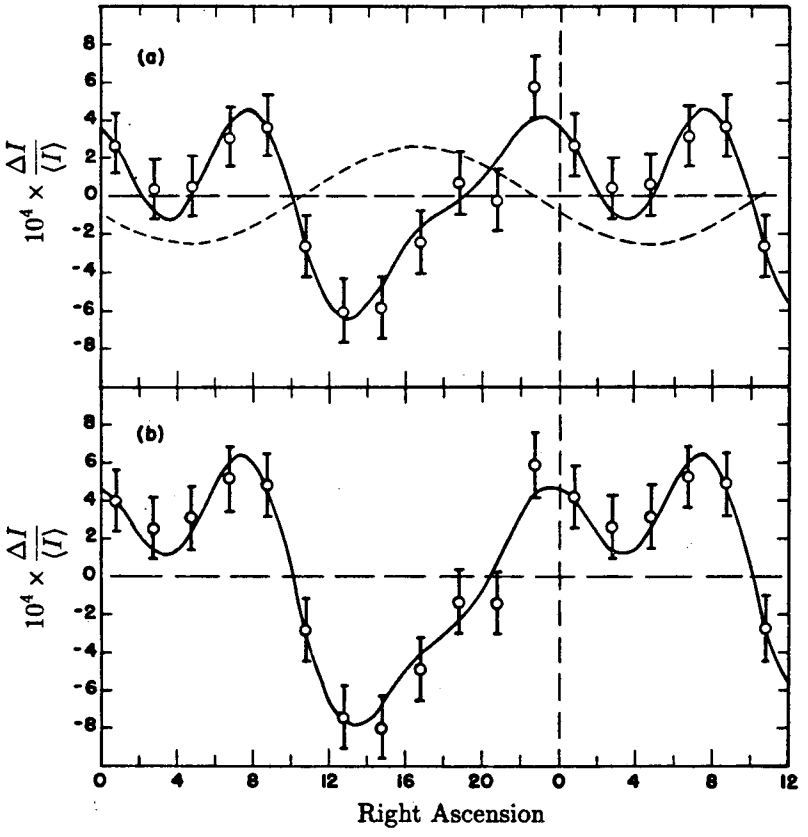

FIG. 7. Folded light curve at the sidereal frequency. In (a) the uncorrected data (solid) and LISM correction (dotted) are shown separately, and in (b) the sum is shown. For clarity, 1.5 periods are shown.

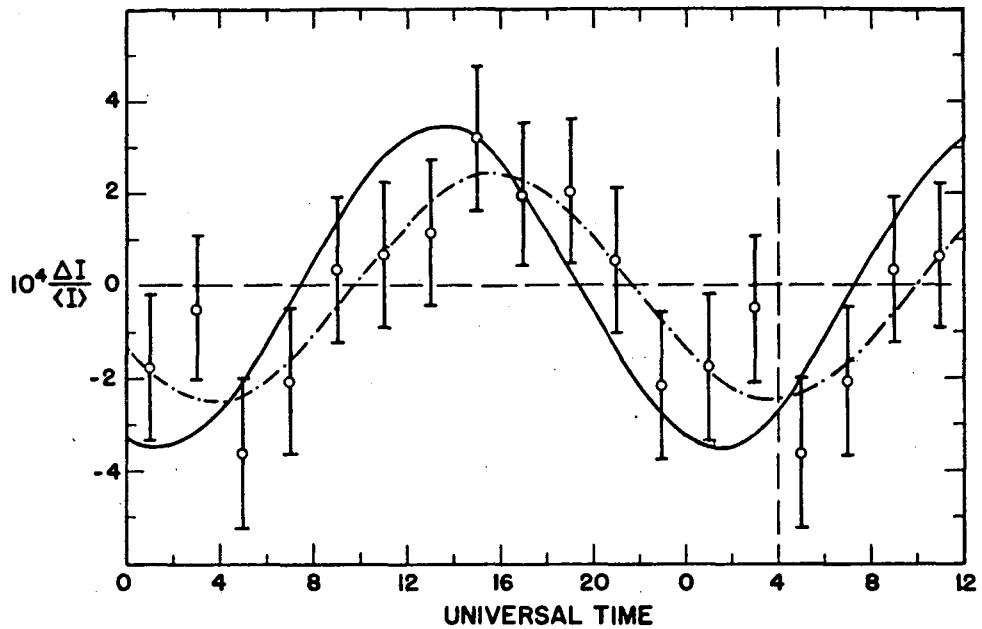

FIG. 8. Folded light curve at the solar frequency.

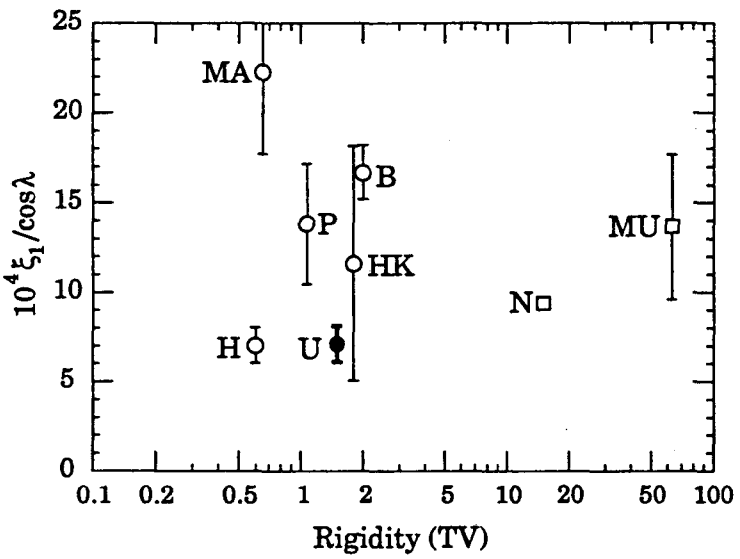

FIG. 9. A comparison of first-harmonic amplitudes obtained with the Utah and other detectors. All results have been corrected for solar motion with respect to the LISM and divided by $\cos\lambda$. Letters by circles indicate underground muon results from Holborn, Matsushiro, Utah, Hong Kong, Baksan, and squares indicate air shower experiments at Mt. Norikura and Musala Peak. Experiments are referenced in the text.

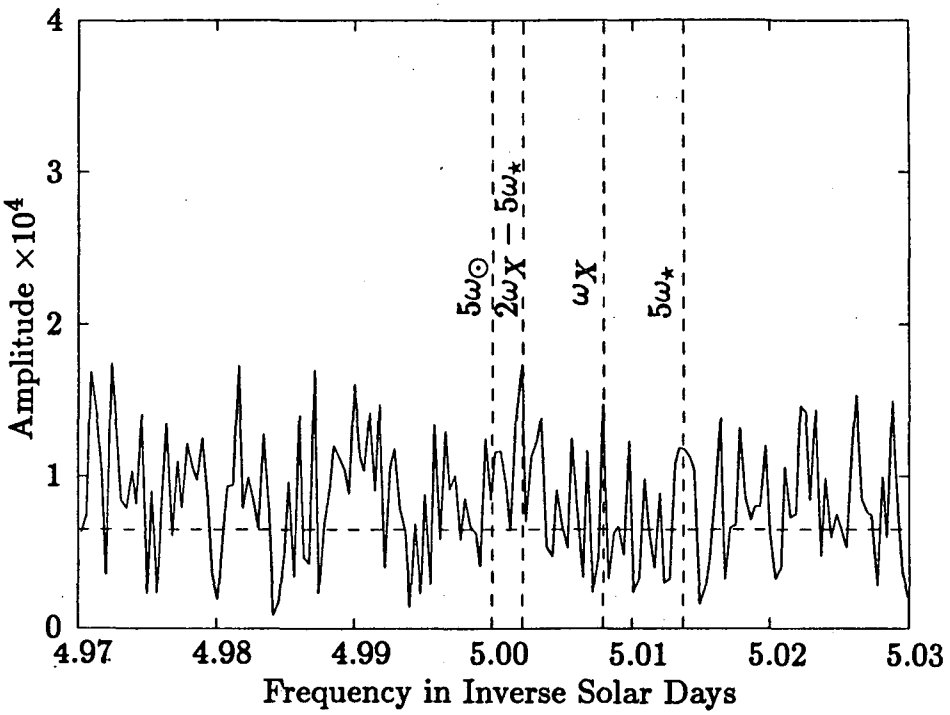

FIG. 10. DFT for data near 5 day^{-1} using data from each sector shifted to enhance the Cygnus X-3 signals at beat frequencies with the sidereal frequency. The vertical lines from left to right correspond to (a) the fifth harmonic of the solar daily frequency, (b) $2\omega_X - 5\omega_\star$, (c) ω_X, the Cygnus frequency, and (d) the fifth harmonic of the sidereal frequency.

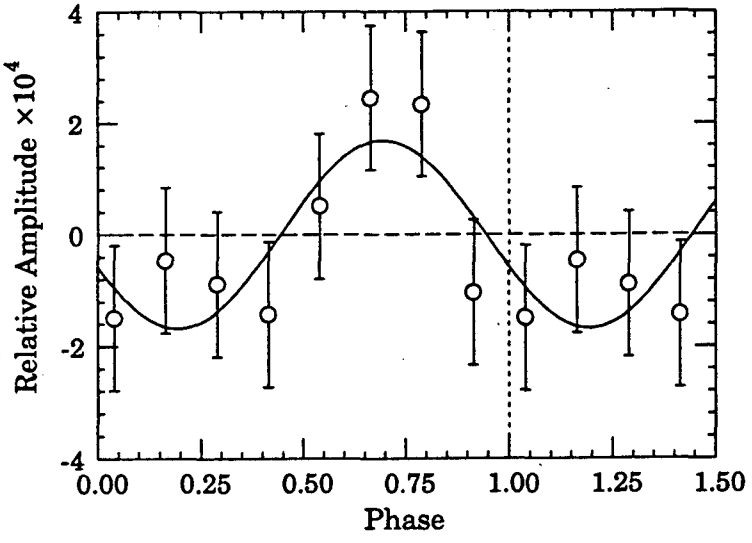

FIG. 11. Folded light curve at the Cygnus period.

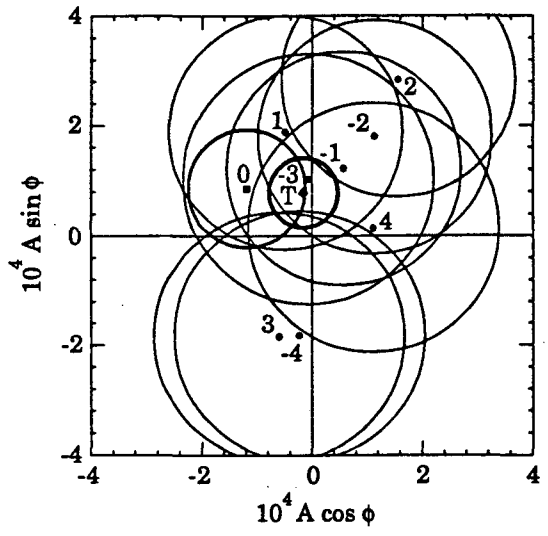

FIG. 12. Real and imaginary parts of the amplitude of the muon signal obtained from the amplitudes of the beat frequencies between Cygnus frequency and multiples of the sidereal frequency. The square dot is the amplitude of the DFT at the Cygnus frequency. The numbered round dots correspond to the DFT amplitudes at frequencies $\omega_X + n\omega_\star$. The diamond represents the weighted combination of all the data. Signals lie within the $1.52\,\sigma$ error circles with 68% probability.

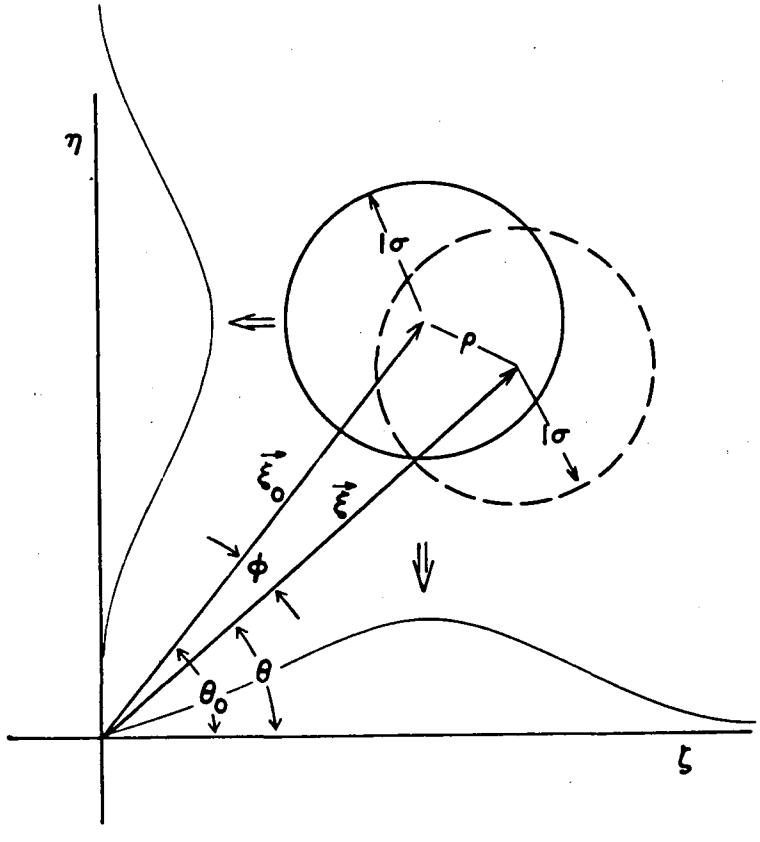

FIG. 13. Definition of variables for the off-center Rayleigh distribution problem.

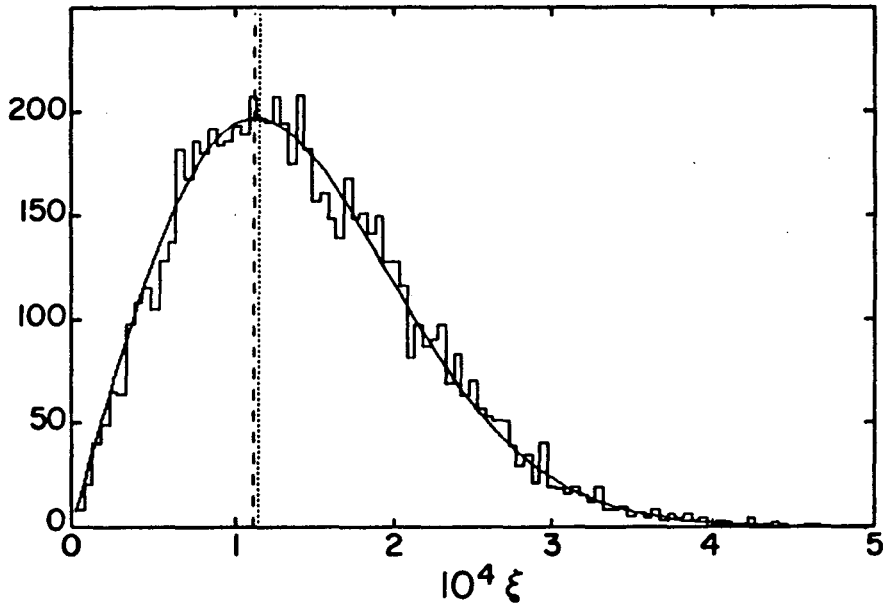

FIG. 14. Distribution of the Fourier amplitude at 7000 frequencies above 0.7 day^{-1} for a partial data set. The solid curve is a Rayleigh distribution with σ adjusted for a best fit. The vertical lines indicate the fitted σ (dashed) and $\sqrt{2/\mathcal{N}}$ (dotted), where $\mathcal{N}$ is the total number of events in the data segment.

LAWRENCE BERKELEY LABORATORY
UNIVERSITY OF CALIFORNIA
INFORMATION RESOURCES DEPARTMENT
BERKELEY, CALIFORNIA 94720